Multiphysics Modeling of Impurity Transport for FNSF Startup Scenario with ERO2.0

Marcos X. Navarro,[a*] Tom Rognlien,[b] Marvin Rensink,[b] Juri Romazanov,[c] Andreas Kirschner,[c] Oliver Schmitz [a]

University of Wisconsin-Madison, Department of Engineering Physics, Madison, WI, USA

Lawrence Livermore National Laboratory, Livermore, CA, USA

Institute of Energy and Climate Research, IEK-4 Forschungszentrum Jülich, Jülich, Germany

*navarrogonza@wisc.edu

Multiphysics Modeling of Impurity Transport for FNSF Startup Scenario with ERO2.0

ABSTRACT

This study focuses on performing a multiphysics study using the ERO2.0 and UEDGE codes for two standard double null configurations for the Fusion Neutron Science Facility: (a) 100% recycling and (b) 99% recycling. Results show that the main contributor to tungsten erosion along the divertor plates are impurities from the midplane waveguides. In addition, the standard high recycling case (100% recycling) shows a significantly higher buildup of impurities along the divertor tiles during the startup phase, which can lead to a higher increase of energy loss in the plasma during steady state operation. Lastly, for high recycling, anomalous diffusion can dominate over parallel field diffusion. The work performed in this study can be iteratively applied to a full operation scenario with additional physics such as those from neutrals, wall shaping and additional external fields.

KEYWORDS: FNSF, ERO2.0, Plasma Wall Interaction, Erosion

I. INTRODUCTION

Plasma material interaction in nuclear environments is a challenging topic and requires modeling the contact of a high-performance edge plasma with materials under radiation impact [1-2]. While this is a complex and highly demanding task, the ERO2.0 code [3] can be used as state-of-the-art PMI modeling tool within the Fusion Nuclear Science Facility (FNSF) conceptualization study [4-6]. The code is equipped with significantly enhanced numerical flexibility to handle large volumes of surfaces and plasma. The model was implemented such that the variety of first wall and divertor choices under discussion can be studied in an iterative way with the plasma edge modeling efforts with UEDGE [7-8] for the FNSF standard double null configuration. An interface has been developed in order to iteratively study particle erosion and impurity transport from plasma facing components for the reactor concept with ERO2.0 from a UEDGE 2D plasma background; in this manuscript, two different recycling startup scenarios for a 20 degree sector are studied.

ERO2.0 [3,9-10] is a fully parallelized three-dimensional kinetic Monte Carlo code capable of modelling full reactor volumes and calculating the desired plasma surface interactions (i.e. physical/chemical erosion and deposition) as well as the transport of the impurities across the volume. SDTrimSP [11] is used to produce a database for the sputter yields for different projectile and target material species. The particle transport step calculates the full particle trajectories, particle re-erosion and re-deposition by following traced impurities eroded during the plasma background erosion step. These test particles then undergo different atomic processes such as ionization and recombination, and their 3D orbits are followed to account for the large forces generated by the surface sheath fields. In addition, the code does not calculate plasma response to the impurities, but rather, it uses the trace impurity approximation, meaning that the particles do not interact with each other or the plasma background due to their low concentration. Because of these capabilities, it is possible to study global erosion and transport of particles present anywhere in the main chamber vessel such as the alloyed copper (Cu/Cr) heating antennas used to sustain the plasma discharge and its impact on the tungsten divertor [12-13].

II. UEDGE CASE SETUP

Plasma backgrounds are required as an input for ERO2.0 to calculate the particle erosion and create test particles for tracing based on the impinging fluxes and energies. These are provided by the UEDGE code, which is used to model the plasma and neutral components as a 2D toroidally symmetric fluids. For the double null configuration used, up-down symmetry is used for the reconstruction. The fixed conditions for these cases are a central magnetic field of B_0=10 T, and the power into the scrape-off layer is held at P_{SOL} = 177 MW for a deuterium/tritium plasma (50:50). The backgrounds use the standard plate recycling coefficient, R_p, of 1.0 and a lower recycling of 0.99, leading to higher ion and electron temperatures on the divertor plates shown in Figure 1. Both cases utilize anomalous radial transport coefficients proportional to R^2, where R is the major radius. This is done to mimic the observed lower turbulence level on the inner portion of the SOL for exact double null plasmas. Both cases in this study exceed steady-state peak heat fluxes on the outer plates in the excess of 20 MW/m^2. These conditions are also associated with high plasma sputtering, particularly for more sensitive components such as waveguides. Therefore, these conditions are tolerated only briefly during start-up.

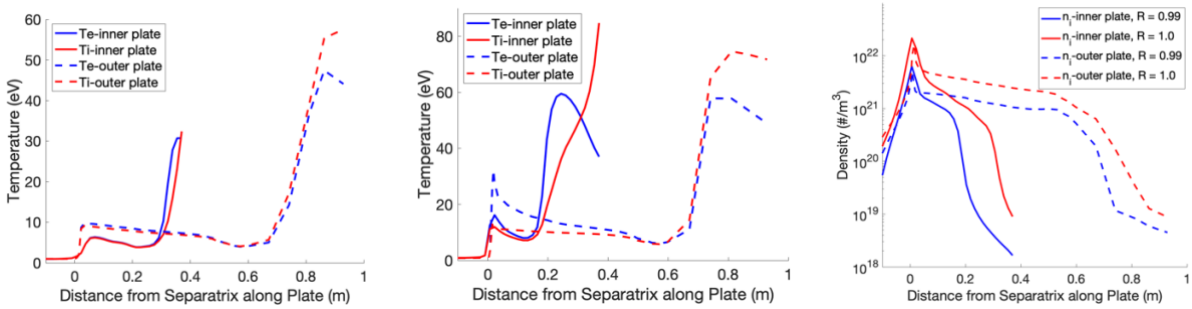

Figure 1. Ion and electron temperatures along divertor plates for the FNSF concept. Setups for (a) high recycling, (b) low recycling, and (c) density profiles across divertor plates of interest are provided by UEDGE on a magnetically aligned grid and converted to ERO2.0 format on a regular grid, and these parameters are used along the corresponding surface cells.

III. ERO2.0 SETUP

This setup utilizes the plasma background from UEDGE from the previous section to study erosion along the divertor plates and the contributions to it due midplane erosion from the copper alloy based current drive antennas for use in FNSF as described in [11]. Due to the low temperatures (Figure 1), tungsten erosion in the divertor from the deuterium and tritium background species (50:50) will be small in the absence of additional impurity species such as neon or nitrogen, which will be expected in a reactor scenario to cool the plasma edge and will also contribute to tungsten sputtering. A cross section of relevant background data is shown in Figure 2. A copper/chromium plate (90:10) is introduced along both the inner and outer midplane locations to simulate the current drive antennas intended to run along the low and high field sides of the vessel chamber. Tungsten plates are used along the upper and lower divertors near the separatrix X-points. For simplicity we don't consider dynamic material mixing with W in the antennas, as no significant amount of tungsten is expected. The divertor plates are defined initially as tungsten, but mixing is considered to determine the impact of the midplane species (Cu/Cr) on W erosion and surface composition. A 10 nm interaction layer is used for the material mixing model. This is used to determine the effect of surface mixing on the net erosion and deposition fluxes, but the penetration depth is not close to real time, as traced particles can gain enough energy during ionization and along the sheath to increase their penetration depth greater than the user-defined inputs. Two-dimensional (2D) cross-field diffusion of traced impurities is varied but is defined as constant throughout the volume. In addition, a boundary is defined by the UEDGE

solution indicated by the red contour on Figure 2, as a collecting boundary due to the lack of a first wall geometry. To avoid particles getting immediately caught by these outer boundaries at the beginning of their trajectory tracing, the plates are moved 0.5 cm into the main plasma. Therefore, future studies should include the use of an onion skin model to extend all plasma parameters from UEDGE to the first wall, to account for any erosion from it, as well as erosion in the first wall from particles from the midplane, and the full current drive antenna geometry along the reactor wall. In addition, these simulations do not include erosion due to high energy charge exchange neutrals, which can contribute significantly to the erosion of the first wall and antenna plates, increasing the amount of particle transport and buildup of impurities along the divertor plates.

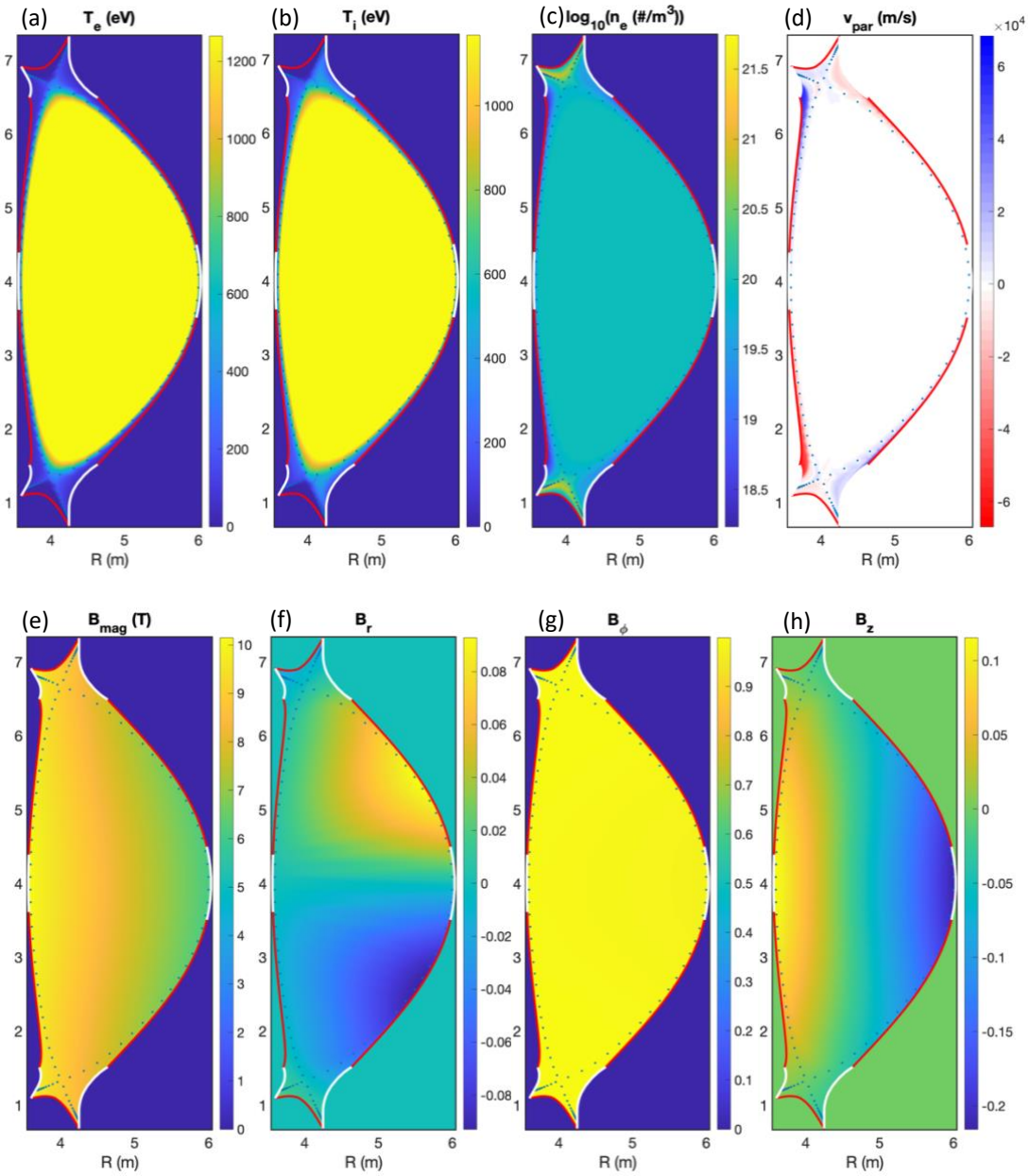

Figure 2. Sample plasma background information for R = 0.99 for (a) electron temperature, (b) ion temperature, (c) plasma density in logarithmic scale, (d) parallel velocity, (e) magnetic field magnitude and directional vectors (f,g,h). The plasma facing components are shown in white, with the tungsten plates at the bottom and top locations, and the copper/chromium plates located at the midplane. The red boundary is used as a collecting boundary for particles exiting the simulation volume and the dotted trace represents the separatrix limit.

High resolution reflection and sputtering yield matrices were generated for these simulations using SDTrimSP [10]. A large number of incident particles were defined (i.e. 100,000 projectiles) were used to calculate the sputter and reflection coefficients to reduce error in these calculations (<1%).

The code uses the Kr-C potential for different surface binding energy models. In the case of gases in Figure 3, the model used utilizes the surface binding energy for the pure material, whereas for solid-solid interactions (i.e. Cu->W) calculates the surface binding energy for the projectile based on the target surface composition as the average of their energies. In addition to the high energy resolution matrix used, the angular dependence was highly resolved at grazing incidence to avoid extreme interpolation at this incidence.

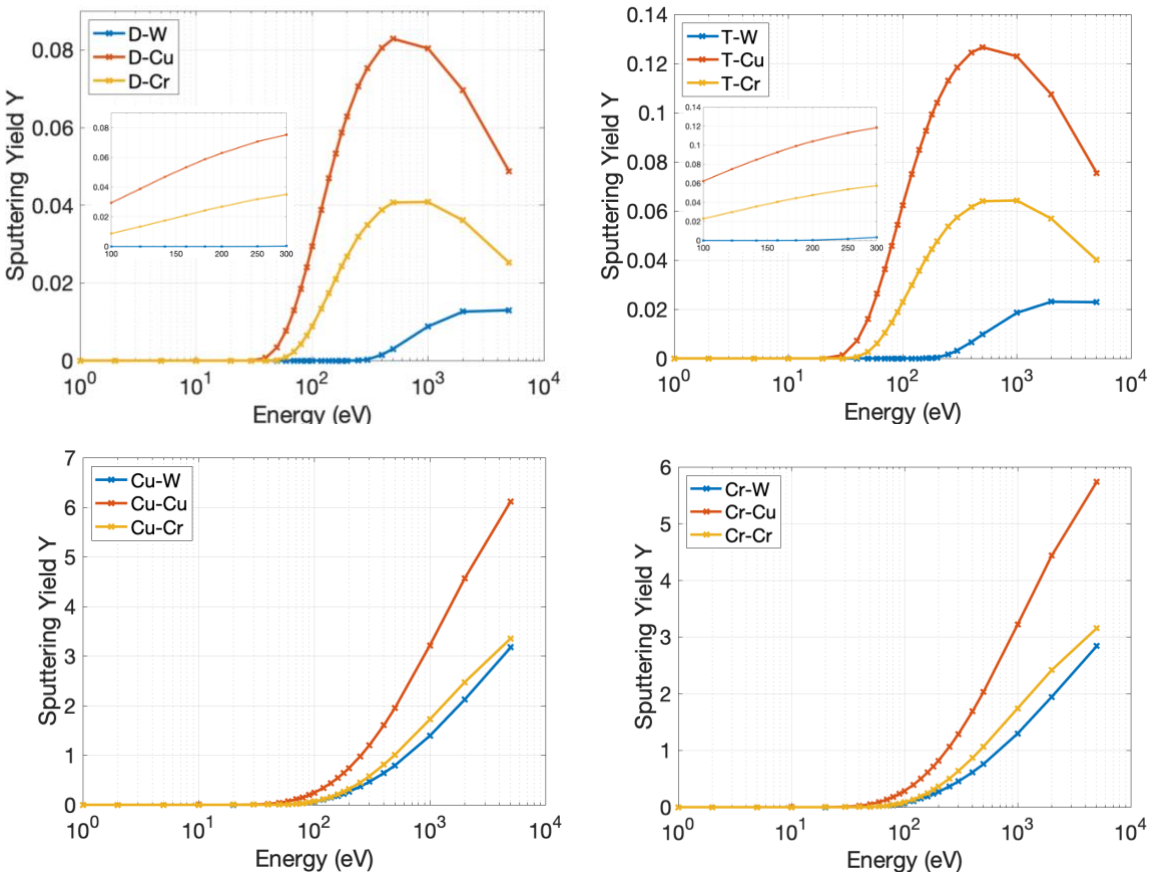

Figure 3. Sputtering yields generated for plasma facing components in the FNSF vessel. Yield matrices use a resolution of 25 energy points and 20 incident angles. The figures shown here correspond to normal incidence. These calculations are highly dependent on the surface binding energy of the target material (e.g. Cu = 3.49 eV, Cr = 4.10 eV, W = 8.79 eV).

IV. RESULTS AND DISCUSSION

Simulations were run for 50 time-steps (dt = 5.0 s) for a total duration of 250 s. The interaction layer used in the homogeneous mixing model calculates particle conservation based on the net particle fluxes from traced particles, and compensates particle depletion from the bulk, and removes excess particles within the layer to the bulk. Erosion and deposition fluxes stabilize after the first few time steps (>10). Midplane impurities (Cu/Cr) are eroded and traced to the lower divertor target on the high field side, and the to the upper divertor target on the low field side as seen in Figure 4. Figure 4a presents the dominating species transport (Cu) in steady state, with its contribution from its higher charge states being the main contributor for the particle deposition in the divertor targets. As the impurities build up their concentration in the divertor targets, they can be re-eroded in sub-sequent steps, leading to the stabilization of the net fluxes on their surfaces. Figures 4b and 4c present the net particle rates along the poloidal direction, starting at the bottom of the lower inner target (on the high field side) and calculated along the clockwise direction for the low recycling case (R_p = 0.99) and the high recycling case (R_p = 1.0) respectively. These profiles show the main impurity deposition zones to be in the lower divertor target (peak 1) on the high field side, the lower midplane region for the antenna plate on the high field side (peak 2), a minimal amount of deposition on the upper divertor plate on the low field side (3), and the upper midplane region for the antenna plate on the low field side (4). Net erosion zones correspond to the upper midplane region for the antenna plate on the high field side and the lower midplane region for the antenna plate on the low field side. Due to the larger ion temperatures at the midplane, larger erosion and deposition rates are observed at the midplane locations for the high recycling case (R_p = 1.0), as well as larger deposition along the divertor target for traced impurities. The integrated tungsten gross erosion fluxes along the divertor tiles due to different sources are summarized in Figure 5 with over 90% of tungsten particles being redeposited across all cases. As expected, due to the low edge temperatures shown in Figure 1, the background contribution to erosion is orders of magnitude smaller than erosion from traced particles from the midplane (Cu/Cr), and tungsten self-sputtering. Among some of the features observed in these profiles is the noticeable increase in W erosion due to midplane impurities for the high recycling case. Additionally, there is a decrease in tungsten self-sputtering, because of its concentration decrease along the surface, and an increased deposition of other impurities (i.e. copper). In addition, erosion

in the upper target is significantly lower than for the inner target, therefore for any subsequent analysis, this study will focus on the lower divertor target.

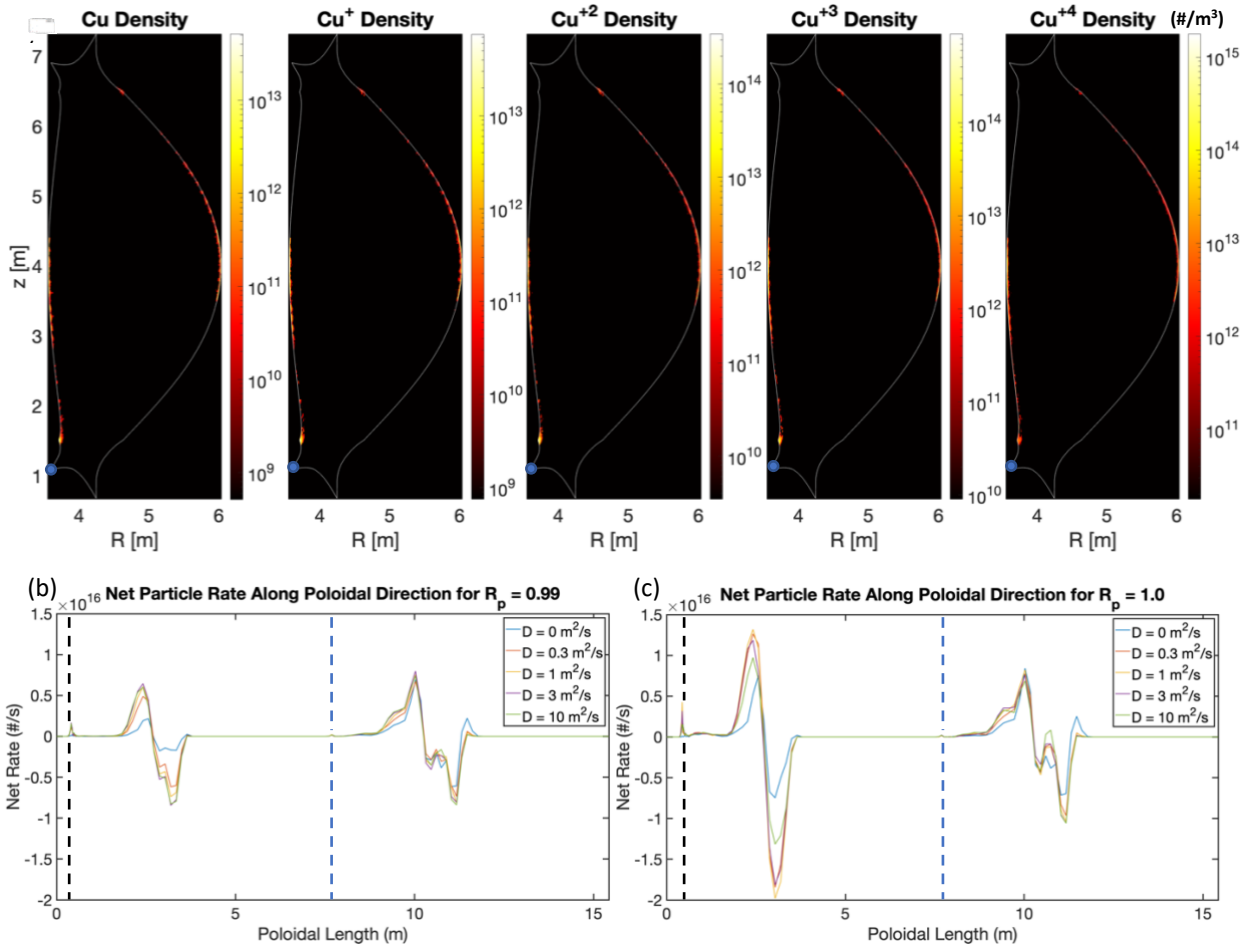

Figure 4. (a) Copper charge state densities for steady state for constant D = 1 m^2/s and a standard recycling scenario of R_p = 1.0. High copper charge state impurities flow from the inner and outer midplane to the lower and upper divertor. Net particle rates (for all species) calculated clockwise along the poloidal direction starting at the bottom of the inner lower divertor target (marked with a blue dot) for (b) R_p = 0.99 and (c) R_p = 1.0. Main strike locations along divertor plates are shown in black dashed lines for the lower divertor, and blue for the upper divertor.

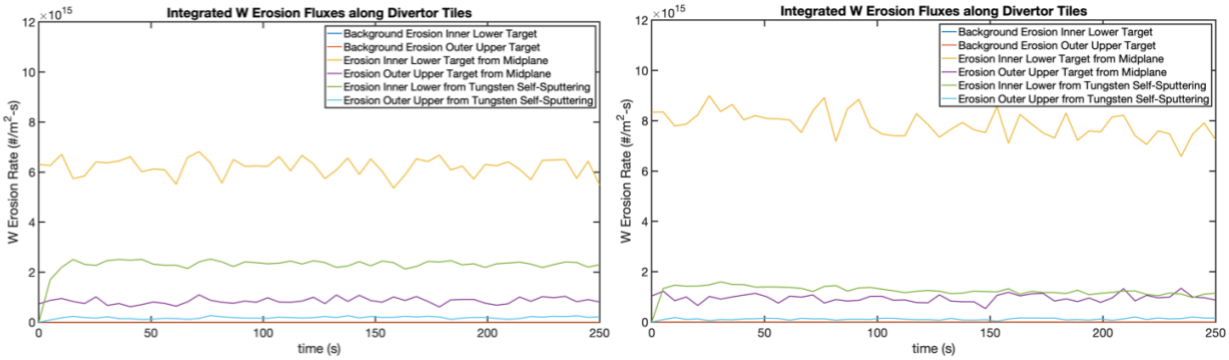

Figure 5. Integrated gross erosion contributions along upper and lower divertor target plates for (a) R_p = 0.99, and (b) R_p = 1.0 for $D_\perp$=1.0 m^2/s. Contributions from background erosion are small compared to W self-sputtering and erosion from trace impurities at the midplane.

The larger particle fluxes coming from the midplane for the high recycling case (Figure 6) contribute to the faster buildup of the impurity layer on the divertor plates and, in tandem with the lower edge temperatures, prevents the erosion of impurity species (Cu/Cr) with lower sputtering thresholds. However, as anomalous (2D cross-field) diffusion is increased, impurity particle deposition in the high recycling case significantly decreases due to particle losses to surface reflection along the target, and across the collecting boundary at the edge of the simulation volume. In the low recycling regime, particles can gain enough energy in the sheath to re-deposit, and re-erode in subsequent steps, leading to a much slower buildup of the concentration of these impurity species, as seen in Figure 7. Because we are using a 2D plasma background, the toroidally averaged time evolution for an anomalous diffusion coefficient of D = 1.0 m^2/s is shown here along the main strike line. This scenario is modeled for the startup period (here ~ 4 minutes), and there is only partial buildup of impurities in the interaction layer during this period for the main strike location on the lower divertor target. For the high recycling scenario, the buildup of copper and chromium is larger by a factor of approximately 3.

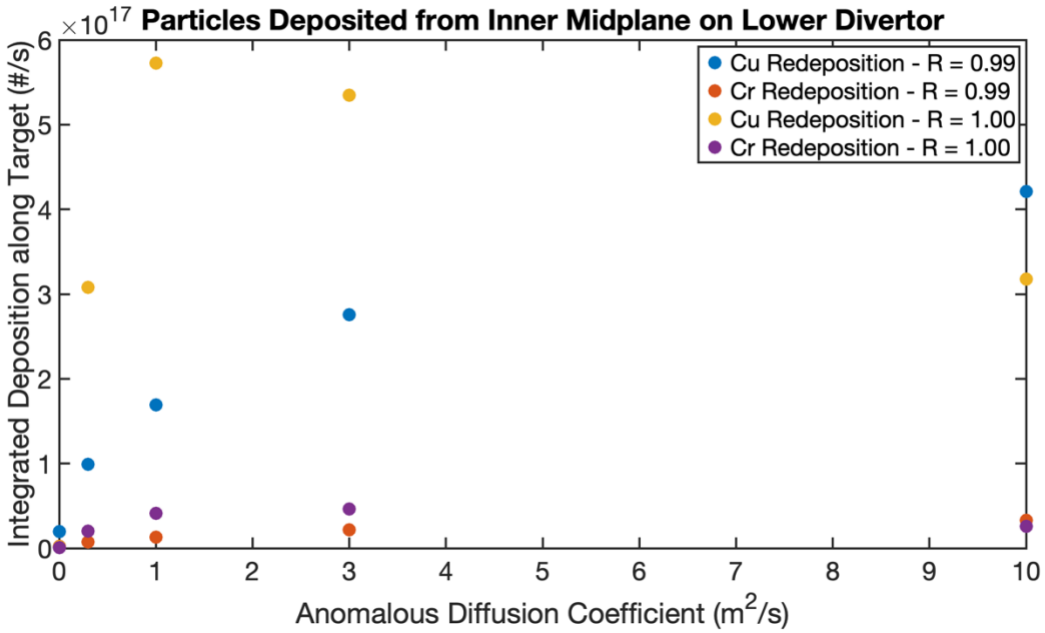

Figure 6. Integrated particle redeposition from the inner midplane to the inner divertor target. A split occurs on particle redeposition as anomalous diffusion is increased.

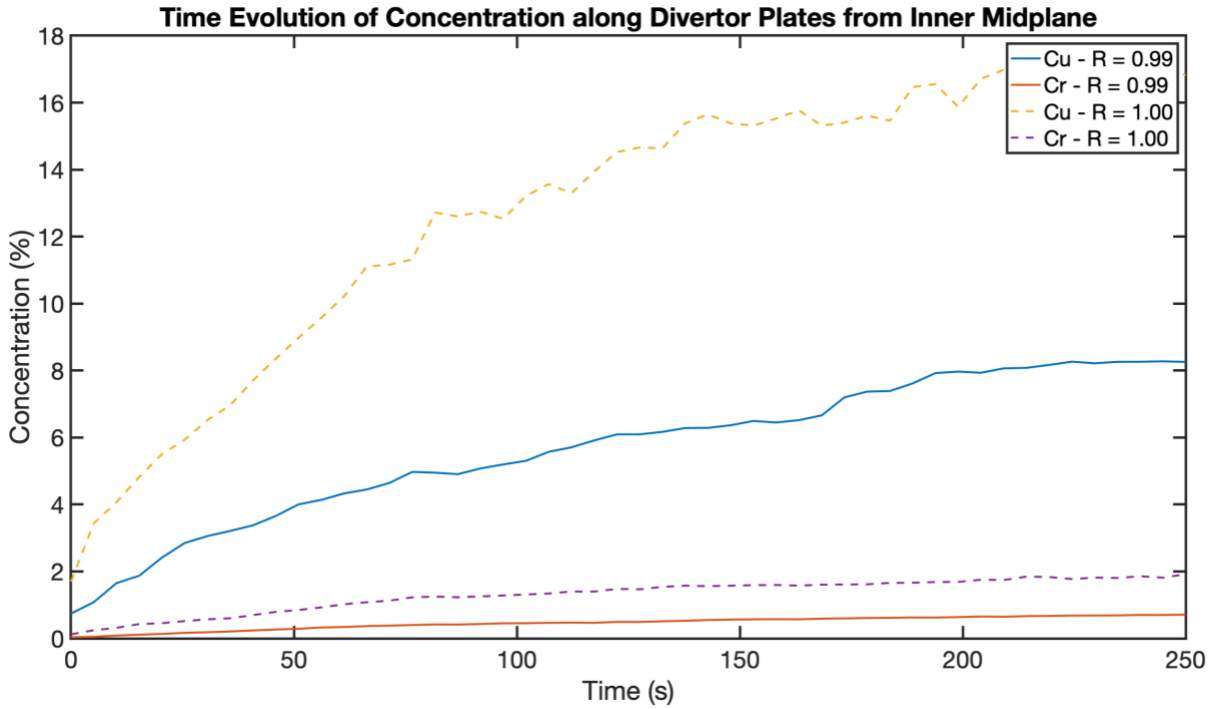

Figure 7. Concentration evolution of copper and chromium along lower divertor target plates for $D_{\perp} = 1.0$ m^2/s. The time evolution shows the toroidal average concentration of the midplane species along a 5 cm strike line. Larger buildup of the species is observed for the high recycling case due to the lower edge temperatures during startup phase.

The concentration of the different impurity species is also dependent on anomalous diffusion (Figure 8), with particle reflection and re-erosion playing a role in the different recycling scenarios as previously discussed. Impurity concentrations along the divertor surface peak for D = 3.0 m^2/s for R_p = 1.0 with copper impurities in the plasma and re-erosion in the divertor plates becoming a potential issue in tungsten erosion for when transitioning from startup to steady state conditions. For low anomalous diffusion values (D < 3.0 m^2/s), particle deposition from midplane impurities increases, as does the total traced impurity erosion (from midplane and target) along the divertor target. In addition, a significant number of impurities are collected at the boundary between the inner midplane and divertor plate during the high recycling discharge. This increase in the traced erosion leads to the lower buildup of copper for D < 3.0 m^2/s, peaking at D = 3.0 m^2/s, and increased losses to the boundary at the boundary for D = 10.0 m^2/s as observed in this case in Figure 9. This is also supported by the higher tungsten erosion along the plate caused by the impurities coming from the midplane (Figure 5). The large differences in the parallel flow velocities between the two cases ((9b) R_p = 0.99, (9c) R_p = 1.0) leads to a small increase in particle losses to the boundary as anomalous diffusion is increased for the high recycling case. Traced impurities coming from the midplane, and traced impurities eroded along the target plate overcome a narrower parallel transport barrier and slower flow velocities near the boundary, leading to impurity particle losses on the order of 10% to the simulation boundary for extreme values of anomalous diffusion (D = 10.0 m^2/s). This dip in concentration is not seen for the low recycling case, where this same increase in anomalous diffusion, leads to particle losses in the order of 3% to the simulation boundary.

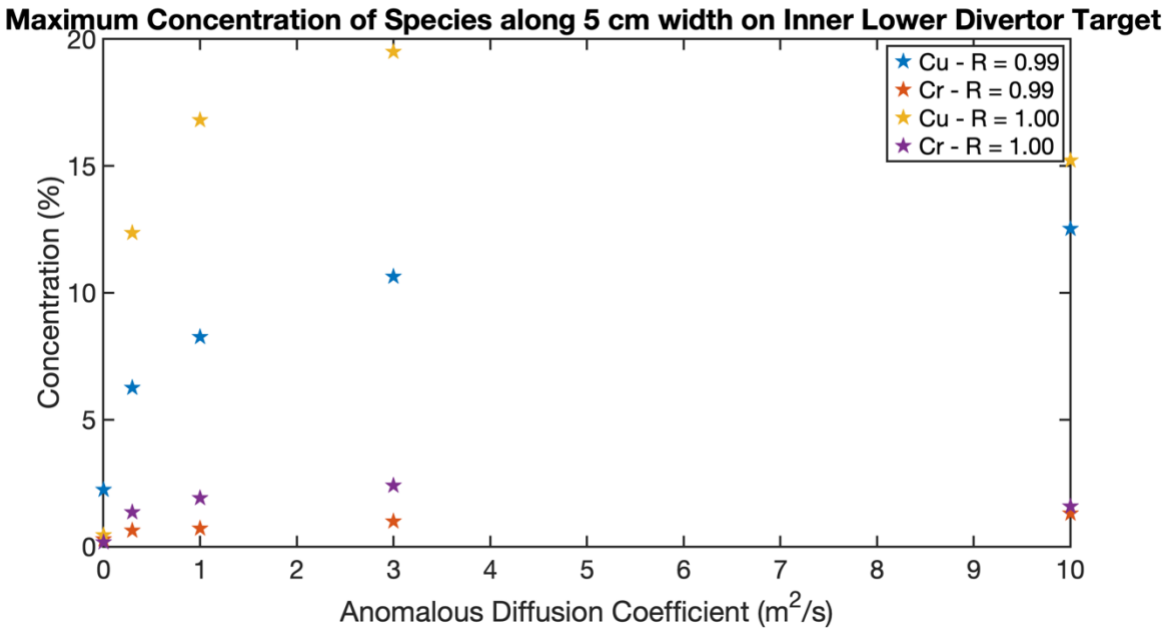

Figure 8. Maximum concentration of impurity species (Cu/Cr) along main buildup region in the lower divertor target as a function of anomalous diffusion.

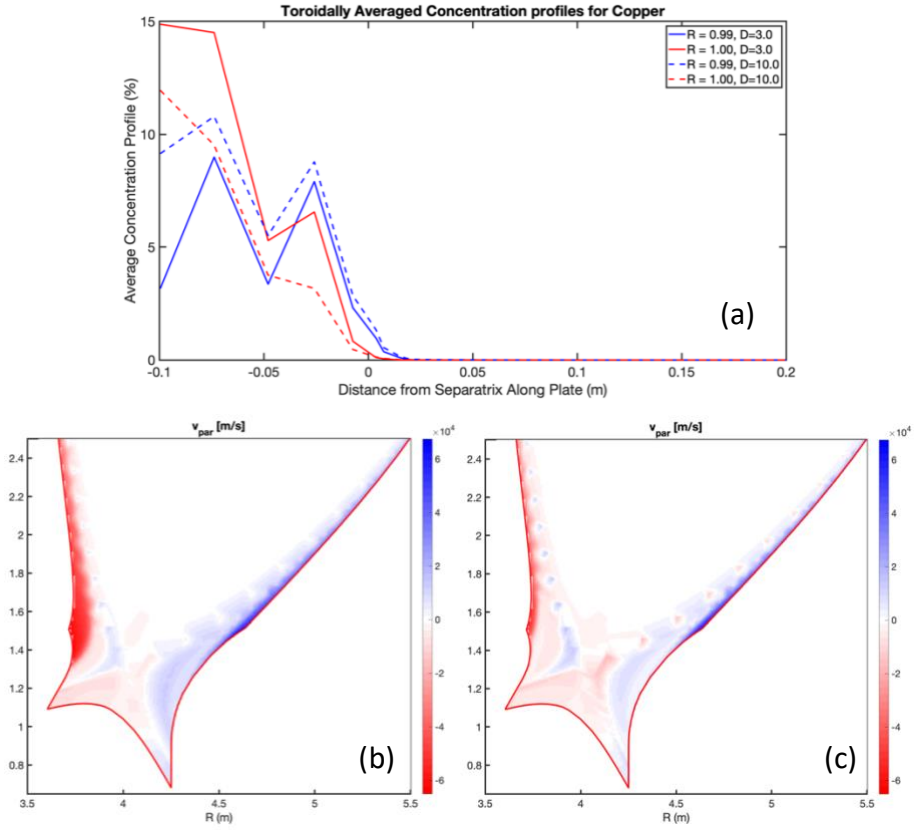

Figure 9. (a) Toroidally averaged copper concentration profiles along a section of the inner lower divertor target for both scenarios. (b) Parallel flow velocity for low recycling (R=0.99). (c) Parallel flow velocity for high recycling (R = 1.0).

Although the cases in this study exceed the allowable steady state heat loads during operation on the outer targets, the ion and electron temperatures in the outer plates are low enough that erosion from the background is negligible. Currently, ERO2.0 does not include the physics for modeling sputtering due to heat spikes, but it is able to provide an initial estimate for impurity sputtering from waveguides, and its contribution to erosion along the divertor targets during the startup phase as presented. Lastly, as previously mentioned, the contributions from high-energy charge exchange neutrals that penetrate to the separatrix region and return to the wall have not been included in the present UEDGE simulations. These will increase wall sputtering of impurities, which can cause these midplane species to be ejected (Cu/Cr), travel deep into the scrape-off layer and contaminate the core. Future efforts could be dedicated to this study as well as the effects of wall shaping once a vessel geometry has been defined.

V. CONCLUSIONS

Results from this study show that midplane erosion is the main contributor to erosion along the divertor plates, with impurity buildup subsequently reducing the amount of tungsten eroded during the FNSF startup phase. Particle transport to the upper divertor targets is significantly smaller than one for the lower targets, requiring an individual lifetime calculation for those divertor tiles. High recycling leads to faster buildup of impurities along the tiles due to the lower plasma edge temperatures. Particle reflection and large differences in the parallel flow velocities across cases affects the particle redeposition as anomalous diffusion increases. For high recycling, cross field diffusion overtakes transport along field lines, leading to particle losses along the simulation boundaries. Full buildup of impurities on the initially tungsten surface along the main deposition regions of the divertor targets is not achieved for these startup conditions but can contribute to erosion and contamination during steady state operation. The inclusion of erosion from charge exchange neutrals will provide a closer estimate to the steady state buildup of these impurities, and its effect on the long-term operation of the device. An iterative analysis can be performed with ERO2.0 and UEDGE, utilizing the PFC's states at the end of each operation point, in addition to a full 3D analysis for the vessel.

VI. ACKNOWLEDGEMENTS

This work was funded in part by the U.S. Department of Energy under grant DE-SC0020284 and DE-SC00013911. This work has been carried out within the framework of the EUROfusion Consortium, funded by the European Union via the Euratom Research and Training Program (Grant Agreement No 101052200 — EUROfusion). Views and opinions expressed are however those of the author(s) only and do not necessarily reflect those of the European Union or the European Commission. Neither the European Union nor the European Commission can be held responsible for them.

VII. BIBLIOGRAPHY

[1] R.A. Pitts et al 2011, "Physics basis and design of the ITER plasma-facing components", Journal of Nuclear Materials 415 (2011) S957–S964, doi:10.1016/j.jnucmat.2011.01.114

[2] A Loarte et al, Transient heat loads in current fusion experiments, extrapolation to ITER and consequences for its operation, Phys. Scr. T128 (2007) 222–228, doi:10.1088/0031-8949/2007/T128/043

[3] J. Romazanov et al, First ERO2.0 modeling of Be erosion and non- local transport in JET ITER-like wall, Phys. Scr. T170 (2017) 014018 (10pp), https://doi.org/10.1088/1402-4896/aa89ca

[4] C.E Kessel et al, Overview of the fusion nuclear science facility, a credible break-in step on the path to fusion energy, 2018 Fusion Eng. and Design 135 (2018) 236-270, https://doi.org/10.1016/j.fusengdes.2017.05.081

[5] A. Davis et al, Neutronics aspects of the FESS-FNSF, 2018 Fusion Eng. and Design 135 (2018) 271-278, https://doi.org/10.1016/j.fusengdes.2017.06.008

[6] A.F. Rowcliffe et al, Materials challenges for the fusion nuclear science facility, Fusion Engineering and Design 135 (2018) 290–301, https://doi.org/10.1016/j.fusengdes.2017.07.012

[7] T.D. Rognlien et al, Scrape-off layer plasma and neutral characteristics and their interactions with walls for FNSF, Fusion Engineering and Design 135 (2018) 380–393, http://dx.doi.org/10.1016/j.fusengdes.2017.07.024

[8] N Christen et al, Exploring drift effects in TCV single-null plasmas with the UEDGE code, Plasma Phys. Control. Fusion 59 (2017) 105004 (15pp), https://doi.org/10.1088/1361-6587/aa7c8e.

[9] J. Romazanov et al, Beryllium global erosion and deposition at JET-ILW simulated with ERO2.0, Nuclear Materials and Energy **18** (2019) 331–338, https://doi.org/10.1016/j.nme.2019.01.015.

[10] J. Romazanov et al, Beryllium erosion and redeposition in ITER H, He and D–T discharges, Nucl. Fusion **62** (2022) 036011 (15pp), https://doi.org/10.1088/1741-4326/ac4776

[11] A. Mutzke et al, SDTrimSP Version 6.00, IPP-Report 2/19, Max Planck Institute for Plasma Physics

[12] G. M. Wallace et al., "Multiphysics Simulations of a Steady-State Lower Hybrid Current Drive Antenna for the FSNF", Fusion Science and Technology, 77:2, 159-171 (2021), DOI: 10.1080/15361055.2020.1858672

[13] G. WALLACE et al., "Heating and Current Drive Actuators Study for FNSF in the Ion Cyclotron and Lower Hybrid Range of Frequency", Fusion Eng. Des., 135, 370 (2018); https://doi.org/10.1016/j.fusengdes.2017.06.025.